

# Characteristics of subzero startup and water/ice formation on the catalyst layer in a polymer electrolyte fuel cell

Shanhai Ge, Chao-Yang Wang\*

*Electrochemical Engine Center (ECEC), and Department of Mechanical and Nuclear Engineering,  
The Pennsylvania State University, University Park, PA 16802, United States*

Received 19 December 2006; received in revised form 18 January 2007; accepted 21 January 2007  
Available online 30 January 2007

## Abstract

This work experimentally explores the fundamental characteristics of a polymer electrolyte fuel cell (PEFC) during subzero startup, which encompasses gas purge, cool down, startup from a subfreezing temperature, and finally warm up. In addition to the temperature, high-frequency resistance (HFR) and voltage measurements, direct observations of water or ice formation on the catalyst layer (CL) surface have been carried out for the key steps of cold start using carbon paper punched with microholes and a transparent cell fixture. It is found that purge time significantly influences water content of the membrane after purge and subsequently cold-start performance. Gas purge for less than 30 s appears to be insufficient, and that between 90 and 120 s is most useful. After gas purge, however, the cell HFR relaxation occurs for longer than 30 min due to water redistribution in the membrane-electrode assembly (MEA). Cold-start performance following gas purge and cool down strongly depends on the purge time and startup temperature. The cumulative product water measuring the isothermal cold-start performance increases dramatically with the startup temperature. The state of water on the CL surface has been studied during startup from ambient temperatures ranging from  $-20$  to  $-1$  °C. It is found that the freezing-point depression of water in the cathode CL is  $1.0 \pm 0.5$  °C and its effect on PEFC cold start under automotive conditions is negligible.

© 2007 Elsevier Ltd. All rights reserved.

**Keywords:** Polymer electrolyte fuel cell; Cold start; Water transport; Catalyst layer; Visualization

## 1. Introduction

The polymer electrolyte fuel cell (PEFC) is widely considered as a promising energy conversion system for the future due to many attributes, among which the principal advantage is the fact that it emits only clean water. However, at a subzero ambient temperature the PEFC produces ice, making the cold-start capability and survivability a great challenge for automotive or outdoor applications. At present, fundamental mechanisms of the subzero startup dynamics are not fully understood, but it is recognized that product water forms ice or frost, accumulating in the cathode catalyst layer (CL), thereby reducing the triple-phase boundary critical for the oxygen reduction reaction and hindering the oxygen diffusion. When the cathode CL is plugged by product ice, a PEFC shuts down. In addition, ice formation and melting in the CL in successive startup and warm up cycles may

induce structural damage to the membrane-electrode assembly (MEA).

Although the cold-start capability and associated MEA durability of a PEFC is critically important, the relevant literature is very scarce and can be roughly divided into three areas: MEA durability from freeze/thaw cycles without water production [1–6], startup dynamics [7–11], and ex situ characterization of Nafion membranes at temperatures below 0 °C [12–14]. Notably, there is controversy on the MEA durability from freeze/thaw cycles and its dependence on the membrane water content in the literature. McDonald et al. [1] observed that the proton conductivity of Nafion 112 membrane does not change and no degradation occurs for the dry MEA subjected to freeze/thaw cycling between  $-40$  and  $80$  °C. Wilson et al. [2] showed that the freezing at  $-10$  °C does not appear to be detrimental to the integrity of MEA even at high water content in the membrane. On the other hand, Cho et al. [3] reported that the performance of a cell containing membrane with high water content is degraded after freeze/thaw cycling between  $-10$  and  $80$  °C. In particular, the electrochemically active area of

\* Corresponding author.

E-mail address: [cxw31@psu.edu](mailto:cxw31@psu.edu) (C.-Y. Wang).

platinum catalyst decreases and the membrane resistance increases. Their later study showed that if the cell is purged with dry gas for 20 min, almost no performance degradation or increase in membrane resistance can be observed after the freeze/thaw cycling [4]. Guo and Qi [5] also observed that while freeze/thaw cycles cause the cathode CL of a fully hydrated MEA to crack, there is no apparent damage to the CL if the cell is purged with dry gases for 1 min. Evidently, purge time is an important factor to determine the membrane water content and hence MEA durability from freeze/thaw cycles. St-Pierre et al. [6] suggested that the optimum purge strategy is to stop the purge operation at a point when water in the channels and gas diffusion layer is removed but water in the membrane is still largely present. He showed that the optimum purge time is 88 s with dry gas at 70 °C and purging of the anode is not necessary. St-Pierre et al. [6] further indicated that if a cell was purged with dry gas at 85 °C (hot purge), progressive performance losses were observed after freeze/thaw cycling. However, in a cell purged with dry gas at 20 °C (cool purge), performance losses were not observed.

To remove product water from the cathode CL and prevent cell shutdown, Kagami et al. [7] proposed to use high-flowrate reactant gases to carry away water vapor through the exhaust. However, the simulation results of Hishinuma et al. [8] showed that cell startup is difficult from temperatures below  $-5^{\circ}\text{C}$  because a large quantity of gas to remove product water would simultaneously take away the heat generated by the cell. Another strategy is to store product water/ice in MEA. Most recently, Oszcipok et al. [9,10] demonstrated that in a cell purged with dry nitrogen prior to freezing, cumulated charge density can reach  $70\text{ C/cm}^2$  (or product water of  $6.5\text{ mg/cm}^2$ ) during a potentiostatic startup from  $-10^{\circ}\text{C}$ . Ice formation in the cathode CL was found to result in both a current density reduction of  $\sim 5.4\%$  (@  $0.45\text{ V}$ ) for each cold start, and a decrease in the electrochemically active surface area of the cathode CL. Mao et al. [11] was among the first to study MEA degradation mechanisms resulting from cold start (i.e. with water production), which is the subject of the present study.

To elucidate the fundamental principles underlying cold start of an automotive PEFC from  $-20^{\circ}\text{C}$  and lower, a series of experimental and modeling studies were published by Wang and co-workers [16–20]. Ge and Wang [16] used a transparent cell and silver mesh GDL to visualize ice formation on the catalyst layer in an operating fuel cell, and showed that the freezing-point depression of water in the CL pores is no larger than  $2^{\circ}\text{C}$ . Therefore, for a practical fuel cell vehicle cold-start that is typically from  $-20^{\circ}\text{C}$  or lower, the freezing-point depression is inconsequential. Mao and Wang [17] delineated the governing physics of water and heat balance in PEFC cold start and presented an analytical model to forecast key parameters such as the initial membrane water content prior to cold start and thermal mass of bipolar plates. Mao et al. [18] further developed a multiphase, transient 3D model to simulate cold-start performance. The model accounted for ice/frost precipitation and growth in the cathode CL and gas diffusion layer (GDL), water transport at very low temperatures, heat transfer with phase transition, oxygen transport, electrochemical kinet-

ics, and their mutual interactions. The 3D numerical model was extensively validated against the experimental data of Tajiri et al. [19,20] with good agreement. Tajiri et al. [19,20] described novel experimental procedures and extensive test data aimed to explore the fundamentals of PEFC cold start.

Continuing this series of studies, in this work we present an experimental study of the complete sequence of PEFC cold start that includes gas purge, cool down, cold startup and warm up. The goal is to elaborate the fundamental characteristics of not only cold startup but also key steps prior to and post cold start. As water or ice formation in these steps holds a key to understanding the fundamental mechanisms involved, a simple but effective method for direct observations in an operating PEFC is devised in this work, along with the measurements of cell high-frequency resistance (HFR), temperature and voltage.

## 2. Experimental

### 2.1. Cell fixture

The cell fixture used in the present work is a transparent PEFC previously developed at ECEC and shown schematically in Fig. 1 [16]. In brief, two gold-plated stainless steel current collector sheets were machined to form a single-path serpentine flowfield with channels 1 mm wide and 0.5 mm deep. A transparent polycarbonate plate was placed outside of the cathode current collector sheet to provide optical access. The polycarbonate plate and anode current collector sheet were clamped by two stainless steel end plates. A window was cut in the cathode end plate for observations. Similarly, a catalyst-coated membrane (CCM) based on an  $18\text{ }\mu\text{m}$  thick Gore-Select membrane was employed. The Pt loadings in the anode and cathode catalyst layers are both  $0.4\text{ mg/cm}^2$ . The active area of the electrode is  $5\text{ cm}^2$ .

A major improvement from the earlier visualization work [16] was that realistic GDLs instead of metal meshes, i.e. two PTFE-proofed carbon papers with microporous layer (20BB, SGL), were employed on both anode and cathode, respectively. The cathode GDL was punched with several holes of about  $400\text{ }\mu\text{m}$  in diameter that are located in various positions of the channel area of the cell. These microholes provide excellent optical access to directly observe water or ice behaviors on the CL surface during cell operation. The use of metal meshes as a model GDL to visualize water behaviors at the catalyst layer surface was described first by Ge and Wang [16] and later by Ishikawa et al. [21]; however, such cells suffer from excessive electric and thermal contact resistances between the CL and the mesh GDL as there is very limited point contact between mesh wires and CL surface. Thus, the previous transparent cells using mesh GDL feature much lower polarization performance during startup, and furthermore, distort the thermal environment due to additional heat generation from the electric contact resistance and artificial temperature distribution inside CL due to thermal contact resistance. The carbon paper GDL punched with microholes overcomes the above described difficulties and preserves the thermal environment, which is a key requirement to accurately portray the events surrounding subzero startup.

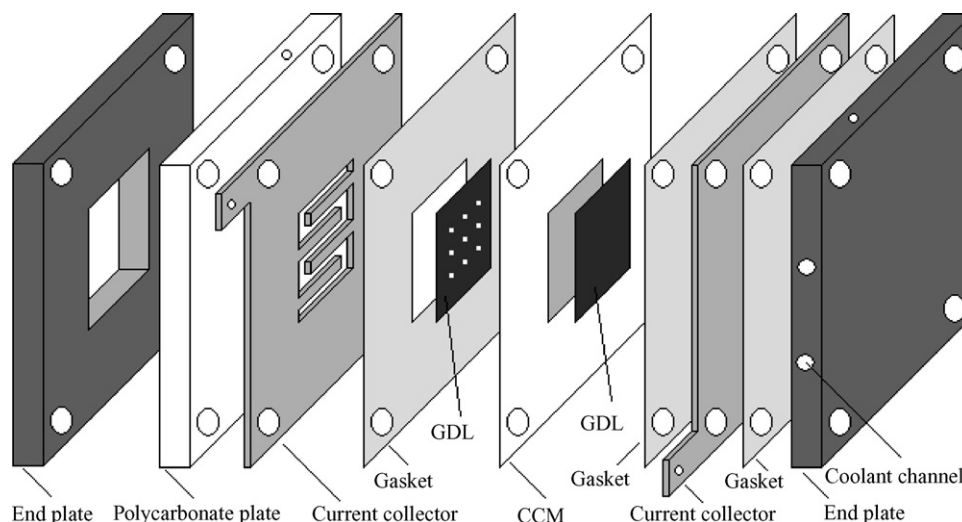


Fig. 1. Schematic of the cell structure. The diameter of the holes punched on cathode carbon paper is about 400  $\mu\text{m}$ .

## 2.2. Experiment procedure and measurements

The experimental cell was connected to a fully computer-controlled fuel cell test station (Arbin Instruments), which regulates the current density and the operating conditions. The pressures of the anode and the cathode were both kept at 1 atm (absolute). The end plate temperature was controlled using a built-in heat exchanger with circulating anti-freeze coolant. The cell was preconditioned by operating it with fully humidified hydrogen and air at low stoichiometric ratios ( $\xi$ ) and at 80 °C for 6 h. Before each purge operation, the cell was operated with fully humidified hydrogen and air at current density of 0.2 A/cm<sup>2</sup>, stoichiometric ratios of 2 and at cell temperature of 55 °C for 30 min. Then both anode and cathode were purged with dry nitrogen at the flow rates of 400 and 900 ml/min under standard temperature and pressure (STP), respectively. The duration of purge varied between 30 and 150 s in this work. During gas purge, the temperatures of the cell and inlet gases were all kept at 55 °C. After purging the cell, the gas inlets and outlets were shut off and the cell temperature was maintained at 55 °C for 32 min to record internal resistance of the cell. Then the coolant was circulated through the end plate to lower the cell temperature to a prescribed startup temperature.

When starting up the cell at a subfreezing temperature, dry hydrogen and air were fed to the cell at stoichiometric ratios of 14.35 and 12.06 (H<sub>2</sub> flow rate: 50 ml/min, STP; air flow rate: 100 ml/min, STP@  $i = 0.1$  A/cm<sup>2</sup>), respectively. The current density was kept constant at 0.1 A/cm<sup>2</sup> (or 0.02 A/cm<sup>2</sup>) during each startup and the cell potential was recorded. When cell potential dropped to 0.1 V, cold startup operation was cut off. Cold startup tests along with in situ imaging were conducted at -20 to -1 °C. After each cold-start operation, the cell was warmed up and then operated with fully humidified hydrogen and air at current density of 1.0 A/cm<sup>2</sup> and at 70 °C for 2 h to restore cell performance. Internal resistance of the cell was recorded during cool down, startup and warm up stages.

A digital camera (Olympus DP 70) combined with a zoom lens (Navitar) were used to record micrographs using external

halogen illumination. The illumination light was turned on only in the period of taking images (1–2 s for each image). HFR measurements (Tsuruga Model 3566 AC Milliohm Meter) were carried out at 1 kHz during all experiments.

## 3. Results and discussion

### 3.1. Gas purge

Purging the cell with dry gases to remove water from the channel, GDL, MPL, CL and membrane is a critical process to create an initial water distribution for subzero startup. We control the purge duration and measure the resulting cell HFR to vary initial water content of the membrane ( $\lambda$ , the number of water molecule per sulfonic acid group) prior to cold start. Fig. 2 shows internal resistances of the cell during and after purge operation. The test sequence is to purge the cell for 150, 120, 90, 60 and finally 30 s. In all the purge tests, the temperatures of the cell and inlet gases were kept at 55 °C. The HFR data generally show that the internal resistance of the cell increases during gas purge, indicating that the membrane and ionomers in the CL are gradually dehydrated by purge gas. More specifically, in situ visualization indicates that in the first 30 s of purge, the purge gas sweeps all water droplets and water film out of the flow channel of the cell. However, residual water in the GDL, MPL and CL remains in this first stage of purge, leading to a rather slow increase in HFR. Between 30 and 150 s of gas purge, the CL and membrane begin to be dehydrated, thus resulting in rapid increase of HFR, as shown in Fig. 2a. This result implies that gas purge shorter than 30 s may not be effective to reduce water content in the membrane in PEFCs.

Once gas purge ceased and the gas inlets and outlets were shut off, all internal resistances of the cell purged with different durations were seen to decrease with time and eventually reach asymptotic values, as shown in Fig. 2b. The decrease in HFR is very rapid in the first 180 s after gas purge and then slows down to reach a steady state at approximately 30 min after purge. This phenomenon is referred to as HFR relaxation in the

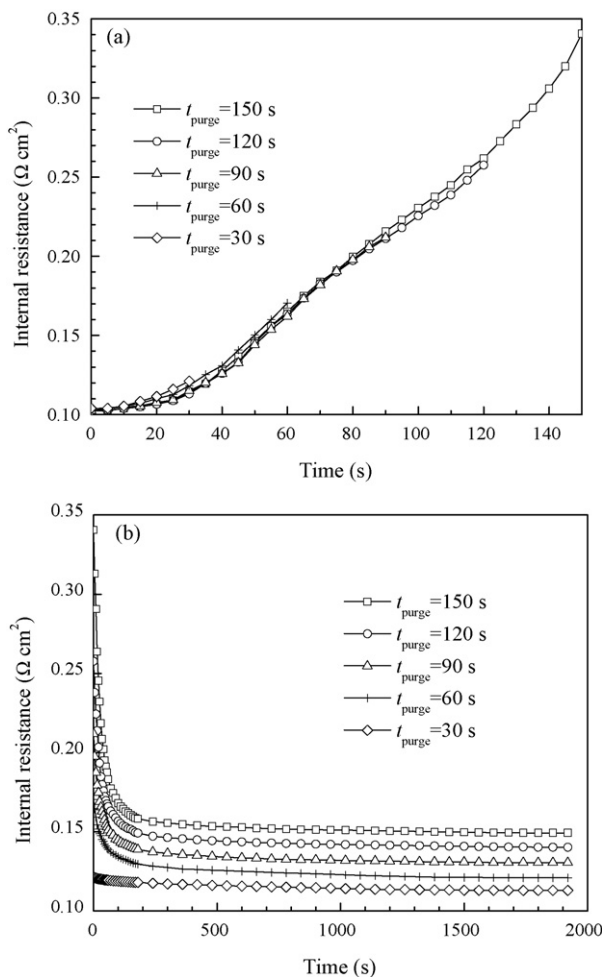


Fig. 2. Internal resistances of the cell (a) during purge and (b) after purge (purge conditions are  $T_{\text{purge}} = 55^\circ\text{C}$ ,  $F_{\text{purge,a}} = 400 \text{ ml/min}$ ,  $F_{\text{purge,c}} = 900 \text{ ml/min}$ . Purge gases are dry nitrogen).

present work. While the measured HFR includes the membrane resistance, CL resistance, and electronic and contact resistances, HFR relaxation obviously originates from the membrane and ionomers. HFR relaxation is a significant feature of gas purge as found for the first time here. While the exact mechanism for HFR relaxation remains elusive, possible explanations include: (1) rehydration of the membrane and ionomers by residual liquid water remaining in pores of CL, MPL and GDL after gas purge; (2) reorganization of the polymer-water structure, particularly in low- $\lambda$  membranes; (3) interfacial non-equilibrium of water between the ionomeric and gas phases [22,23]; and (4) internal diffusion of water inside the membrane. The last reason due to internal diffusion within the membrane becomes less likely for medium to high water content as the diffusion time constant is scaled with  $(\delta_m^2/D_w)$ , where  $\delta_m$  is the membrane thickness and  $D_w$  the water diffusivity estimated to be  $2.2 \times 10^{-6} \text{ cm}^2/\text{s}$  for Gore-Select membranes at water content of 6.0 and at  $55^\circ\text{C}$  [24,25]. Thus, the diffusion time constant is estimated to be  $\sim 1.5 \text{ s}$ , much shorter than that of HFR relaxation. Further investigation on HFR relaxation after gas purge is needed as it dramatically reduces the effectiveness of gas purge during shutdown and cool down of a fuel cell vehicle.

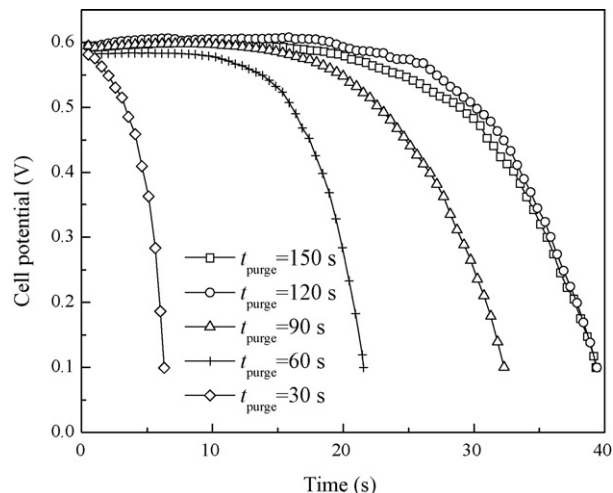


Fig. 3. Cell voltage curves for startup from  $-20^\circ\text{C}$  with different purge times (startup conditions are  $T_{\text{cell}} = -20^\circ\text{C}$ ,  $i = 0.1 \text{ A/cm}^2$ ,  $\xi_{\text{H}_2} = 14.35$ ,  $\xi_{\text{air}} = 12.06$ ,  $\text{RH}_{\text{H}_2} = \text{RH}_{\text{air}} = 0\%$ ,  $p_{\text{H}_2} = p_{\text{air}} = 1 \text{ atm}$ ).

### 3.2. Cold start

After purging the cell and then holding at  $55^\circ\text{C}$  for 32 min to stabilize the cell HFR, the cell was cooled down to  $-20^\circ\text{C}$  in preparation for cold start. Dry hydrogen and air were fed to the cell and the current density was kept constant at  $0.1 \text{ A/cm}^2$  in all startup experiments. The test cell possessed excessive thermal mass such that the cell temperature did not rise during cold start, i.e. isothermal cold start; however, the cumulative product water till cell shutdown is indicative of the intrinsic cold-start capability of a MEA [16,18,19]. Fig. 3 shows cell voltage curves for startup from  $-20^\circ\text{C}$  for purge durations ranging from 30 to 150 s. It is seen that the operational time during cold start increases with the purge duration. This is due to the fact that some product water generated during cold start is transported into the initially dry membrane caused by gas purge, thus postponing the plugging of the cathode CL by ice or frost and hence voltage drop-down. For initially drier membranes resulting from purge of longer duration, it can be seen that upon start, the cell voltage initially increases slightly as the dry membrane absorbs water and hence improves its conductivity. For the cell purged with dry gases for 30 s, the initial increase in cell voltage does not exist as the membrane remains nearly fully hydrated after short purge. Note also from Fig. 3 that the difference in cold-start performance between 120 and 150 s purge diminishes, thus suggesting the existence of optimal purge duration.

Fig. 4 displays initial water content of the membrane prior to cold start and the amount of product water generated during cold start for different purge times. The product water ( $m_w$ ,  $\text{g/cm}^2$ ) can be simply calculated from

$$m_w = \frac{it}{2F} M_w \quad (1)$$

where  $t$  is operational time prior to cutoff voltage,  $i$  the current density,  $F$  Faraday's constant, and  $M_w$  the molecular weight of water. The initial water content of the membrane is estimated from the measured HFR at  $30^\circ\text{C}$  based on the membrane

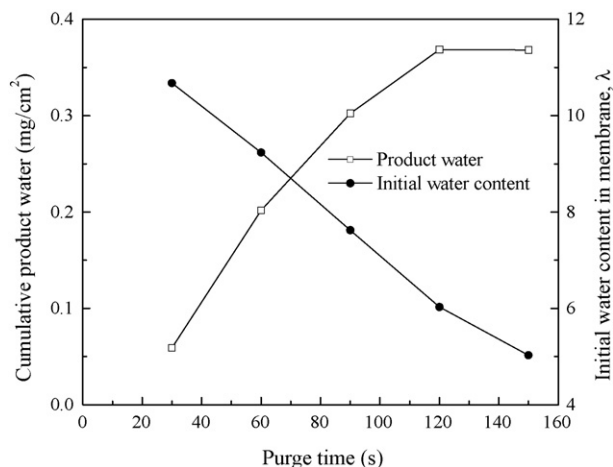


Fig. 4. Water content of the membrane after purge and the cumulative product water during cold start for the cell purged with dry gases for different durations. Water content of the membrane is calculated from the cell resistance at 30 °C (startup conditions are  $T_{\text{cell}} = -20$  °C,  $i = 0.1$  A/cm<sup>2</sup>,  $\xi_{\text{H}_2} = 14.35$ ,  $\xi_{\text{air}} = 12.06$ ,  $\text{RH}_{\text{H}_2} = \text{RH}_{\text{air}} = 0\%$ ,  $p_{\text{H}_2} = p_{\text{air}} = 1$  atm).

conductivity-water content relationship of Springer et al. [26] It can be seen from Fig. 4 that the initial water content of membrane decreases almost linearly with purge duration and the cumulative product water during cold start increases with increasing purge duration or decreasing membrane water content. As explained earlier, the product water reaches a plateau at low water content or for purge time between 120 and 150 s.

It is worthy comparing gas purge conditions employed in various studies. Cho et al. [4] reported that their cell was purged with dry gas for 20 min, while St-Pierre et al. [6] suggested that the optimum purge time was only 88 s and purging of the anode was not necessary. Cho et al. [4] and St-Pierre et al. [6] did not study the effect of purge conditions on cold-start performance. Oszcipok et al. [9,10] reported that their purging process continued until the internal resistance of the cell increased to values large than 23  $\Omega$  cm<sup>2</sup>. This is about two orders of magnitude higher than that studied here. It is obvious that the membrane was extremely dry in Oszcipok's work.

Effects of startup temperature were experimentally explored. Fig. 5 shows cell voltage curves for startup from  $-20$ ,  $-15$ ,  $-10$ ,  $-5$ ,  $-4$ ,  $-3$  and  $-1$  °C. As shown above, the performance of cold start from  $-20$  °C is optimal when the cell is purged with dry gases for 120 s. Thus, 120 s purge duration was used throughout startup from  $-15$ ,  $-10$ ,  $-5$ ,  $-4$ ,  $-3$  and  $-1$  °C, and the current density was set to 0.1 A/cm<sup>2</sup>. Strikingly, Fig. 5 illustrates that the operational time depends strongly on the startup temperature, with the startup from  $-1$  °C proceeding indefinitely without shutdown. Fig. 6 shows the corresponding HFR evolutions during these startup experiments. By and large, the cell internal resistance decreases as the membrane takes up product water during cold start. For startup from  $-1$  to  $-10$  °C, the internal resistance appears to stabilize after a certain period of cold start.

The amount of product water in each startup is correlated with the startup temperature in Fig. 7. It is shown that the cumulative product water at cell shutdown improves modestly for the

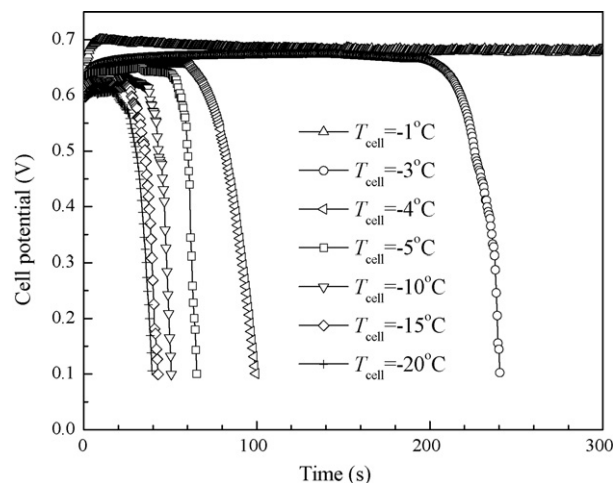


Fig. 5. Cell voltage curves for startup from  $-20$ ,  $-15$ ,  $-10$ ,  $-5$ ,  $-4$ ,  $-3$  and  $-1$  °C (purge conditions are  $T_{\text{purge}} = 55$  °C and  $t_{\text{purge}} = 120$  s, and startup conditions are  $i = 0.1$  A/cm<sup>2</sup>,  $\xi_{\text{H}_2} = 14.35$ ,  $\xi_{\text{air}} = 12.06$ ,  $\text{RH}_{\text{H}_2} = \text{RH}_{\text{air}} = 0\%$ ,  $p_{\text{H}_2} = p_{\text{air}} = 1$  atm).

temperature range of  $-20$  to  $-5$  °C, but drastically increases for startup temperatures higher than  $-5$  °C. In particular, at the startup temperature of  $-3$  °C, the cell can be operated for  $\sim 240$  s. That indicates that the waste heat generated during startup from  $-3$  °C is sufficient to keep the CL and GDL above the freezing point. The amount of product water from startup at  $-3$  °C is 2.24 mg/cm<sup>2</sup>, which is higher than the theoretical water storage capacity of the membrane and cathode CL combined (i.e. 0.85 mg/cm<sup>2</sup> as estimated from the previous work [16]). This means that a portion of the product water must have transported into the MPL or GDL. In comparison, the amount of product water during startup from  $-5$  °C is 0.59 mg/cm<sup>2</sup>, lower than the theoretical water storage capacity of the membrane and cathode CL. This implies that the cathode CL temperature is below 0 °C and part of product water probably forms ice or frost so as to plug and shut down the CL.

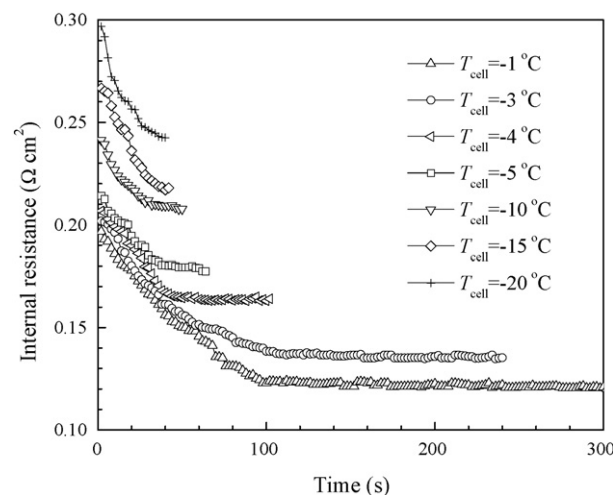


Fig. 6. Internal resistance of the cell during cold start from different temperatures (purge conditions are  $T_{\text{purge}} = 55$  °C,  $t_{\text{purge}} = 120$  s, and startup conditions are  $i = 0.1$  A/cm<sup>2</sup>,  $\xi_{\text{H}_2} = 14.35$ ,  $\xi_{\text{air}} = 12.06$ ,  $\text{RH}_{\text{H}_2} = \text{RH}_{\text{air}} = 0\%$ ,  $p_{\text{H}_2} = p_{\text{air}} = 1$  atm).

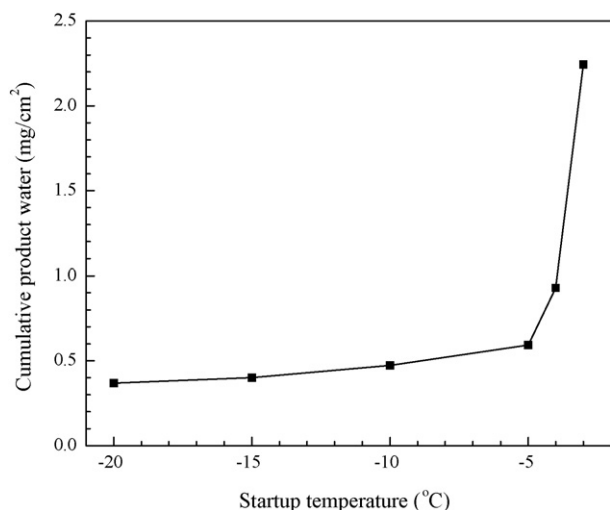


Fig. 7. Cumulative product water during cold start from different startup temperatures (purge conditions are  $T_{\text{purge}} = 55^\circ\text{C}$  and  $t_{\text{purge}} = 120\text{ s}$ , and startup conditions are  $i = 0.1\text{ A/cm}^2$ ,  $\xi_{\text{H}_2} = 14.35$ ,  $\xi_{\text{air}} = 12.06$ ,  $\text{RH}_{\text{H}_2} = \text{RH}_{\text{air}} = 0\%$ ,  $p_{\text{H}_2} = p_{\text{air}} = 1\text{ atm}$ ).

### 3.3. Cool down and warm up

The cool down and warm up processes prior to and post cold start have significant implications to cold-start performance and MEA durability. Moreover, these two processes are of main concern in freeze/thaw cycling studies. Fig. 8 shows the temperature dependences of the cell HFR during cool down after purge of various duration and holding of 32 min at  $55^\circ\text{C}$  as well as during subsequent warm up after cold start. The cooling and heating rates were approximately  $0.5$  and  $1.0^\circ\text{C}/\text{min}$ , respectively. During cool down, it is interesting to find that the cell HFR smoothly increases for purge durations of 90–150 s (or equivalently membrane water content between 5.0 and 7.6 according to Fig. 4). However, for purge duration of 60 s (or membrane water content of 9.2), there exists a point of deflection at about  $-10^\circ\text{C}$  on the HFR-temperature curve, signifying a phase transition of water within the membrane. The same point of deflection occurs at  $-7^\circ\text{C}$  for purge duration of 30 s or membrane water content of 10.7. It is well known that the phase transition of water in the membrane occurs at different subzero temperatures, depending on the water content [12–15,19]. Additionally, Fig. 8 suggests that water freezing in the membrane can be avoided by purging a PEFC between 90 and 120 s prior to cool down. For 30 s purge, the internal resistance is highest when the cell temperature decreases to  $-20^\circ\text{C}$ .

Fig. 8b shows the internal resistance evolutions during warm up after cold start. Prior to warming up, the residual hydrogen and air on the anode and cathode sides of the cell were replaced by nitrogen. Current load was turned off and inlet and outlet gases were shut off. The cell was then warmed up at a rate of  $1.0^\circ\text{C}/\text{min}$ . All the internal resistances of the cell purged with different times are seen to decrease sharply around  $0^\circ\text{C}$ , corresponding to ice thawing in the CL and membrane. The reason is that ice generated during cold startup melts at about  $0^\circ\text{C}$ . Comparing Fig. 8a and 8b, it is found that the internal resistance of the cell at  $-20^\circ\text{C}$  post cold start was higher than

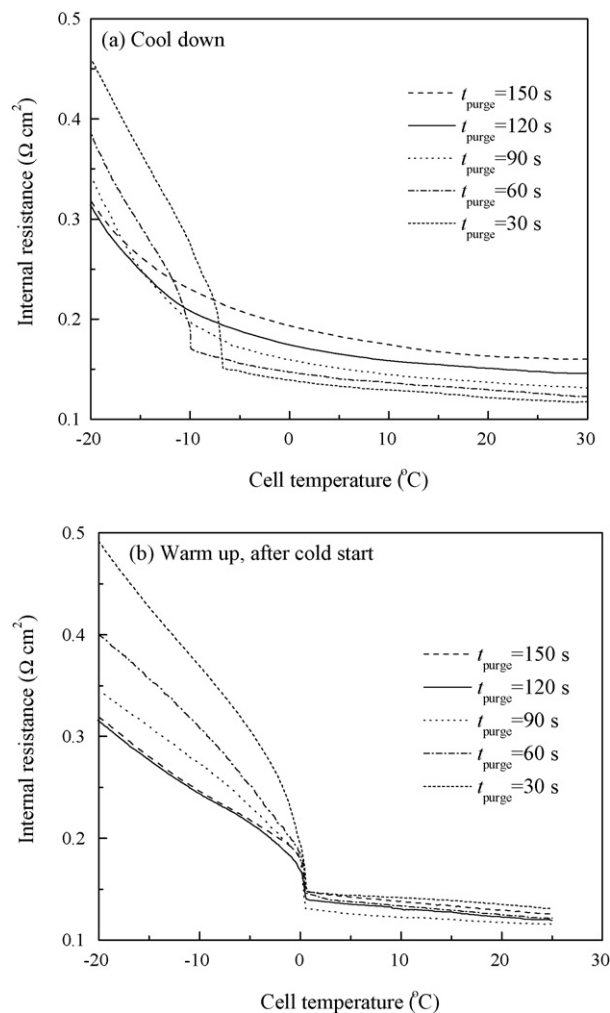


Fig. 8. Internal resistances during (a) cool down and (b) warm up for the cell purged with different durations.

that prior to it. On the other hand, the cell resistance at  $20^\circ\text{C}$  post cold start and after warm up was generally lower than that prior to cold start at  $20^\circ\text{C}$ . This can be explained by the fact the water production during cold start and subsequent ice melting during warm up results in membrane hydration and hence lower resistance than prior to cold start and after gas purge.

### 3.4. Visualization of water/ice formation on catalyst layer

To understand the dependence of product water on the startup temperature, it is instructive to visualize the water or ice formation on the CL surface during cold start. Fig. 9 shows a series of such images from a single microhole of the cathode GDL during startup from  $-1^\circ\text{C}$ . The view in Fig. 9 (and Figs. 11 and 12) is located in the center of the flowfield. The microhole is marked by a dash-line ring in these images for better viewing.

Recall that the cell can operate indefinitely at  $-1^\circ\text{C}$  as shown in Fig. 6. Fig. 9a and b show that no water appears on the surface of CL when the cumulative product water reaches  $0.84\text{ mg/cm}^2$ . Liquid water in the form of droplets begins to appear as the cumulative product water becomes  $1.12\text{ mg/cm}^2$ ; see Fig. 9c. To interpret these experimental observations, it is useful to con-

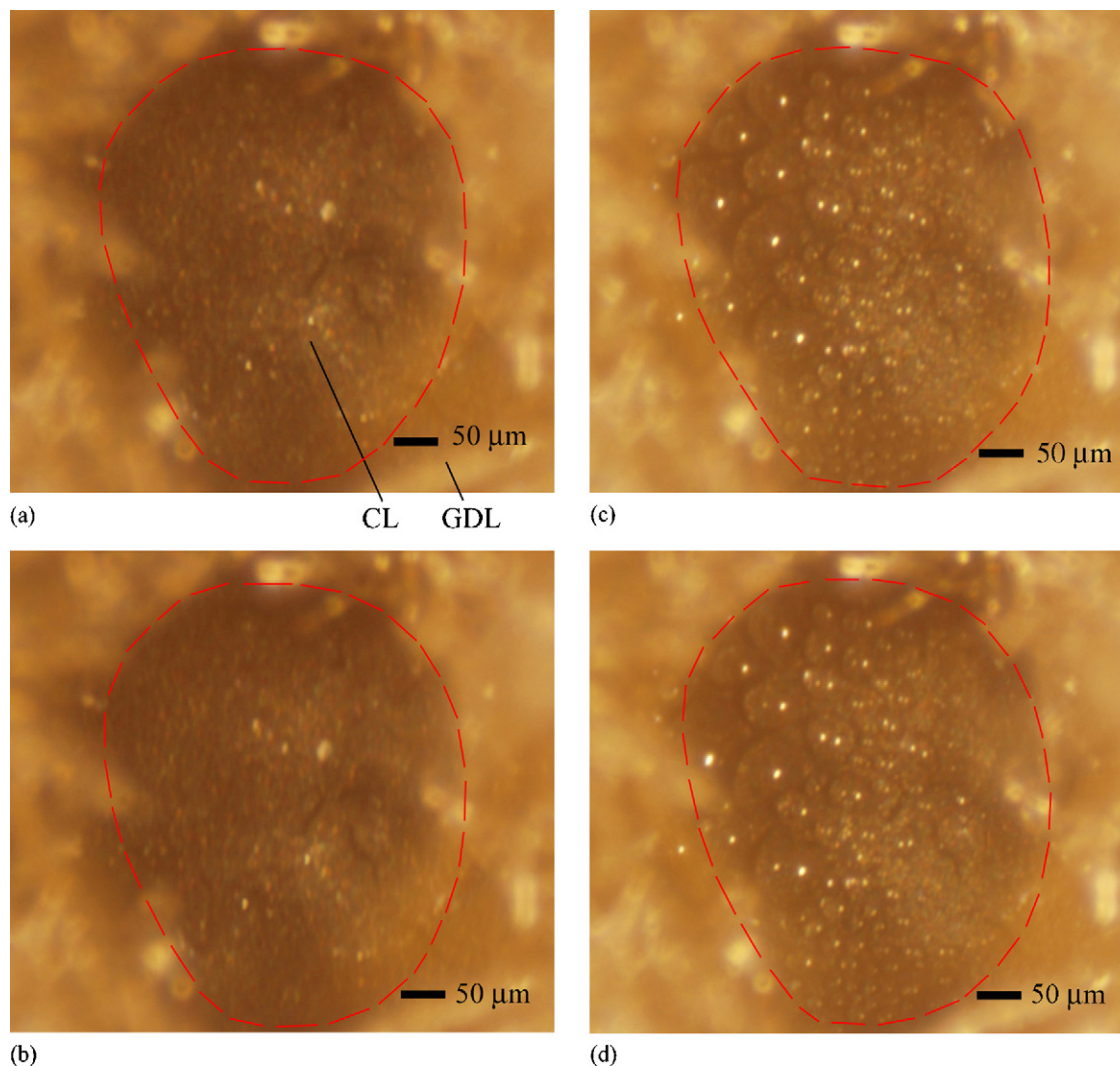


Fig. 9. Images on the CL surface during startup from  $-1\text{ }^{\circ}\text{C}$  (purge conditions are  $T_{\text{purge}} = 55\text{ }^{\circ}\text{C}$ ,  $t_{\text{purge}} = 120\text{ s}$ , and startup conditions are  $T_{\text{cell}} = -1\text{ }^{\circ}\text{C}$ ,  $i = 0.1\text{ A/cm}^2$ ,  $\xi_{\text{H}_2} = 14.35$ ,  $\xi_{\text{air}} = 12.06$ ,  $\text{RH}_{\text{H}_2} = \text{RH}_{\text{air}} = 0\%$ ,  $p_{\text{H}_2} = p_{\text{air}} = 1\text{ atm}$ ). The dashed line outlines the peripheral of the microhole. (a)  $m_w = 0\text{ mg/cm}^2$ ,  $m_w = 0.84\text{ mg/cm}^2$ , (c)  $m_w = 1.12\text{ mg/cm}^2$  and (d)  $m_w = 2.24\text{ mg/cm}^2$ .

sider water transport mechanisms during startup. First, part of water produced by ORR in the cathode CL can be removed by reactant gases exiting the cell. The remainder of product water then accumulates inside the cell. The molar flow rate of water leaving the cell ( $F_{\text{w,out}}$ , mol/s) through the exhaust gas can be estimated by

$$F_{\text{w,out}}^{\text{a}} = \left( F_{\text{H}_2} - \frac{iA}{2F} \right) \frac{p_{\text{w}}^{\text{a}}}{p^{\text{a}} - p_{\text{w}}^{\text{a}}} \quad (2)$$

$$F_{\text{w,out}}^{\text{c}} = \left( F_{\text{Air}} - \frac{iA}{4F} \right) \frac{p_{\text{w}}^{\text{c}}}{p^{\text{c}} - p_{\text{w}}^{\text{c}}} \quad (3)$$

where  $F_{\text{H}_2}$  and  $F_{\text{air}}$  are the molar flow rates (mol/s) of hydrogen and air entering the cell, respectively,  $A$  the active area of the electrode,  $p^{\text{a}}$  and  $p^{\text{c}}$  the gas pressures (Pa) of the anode and cathode, and  $p_{\text{w}}^{\text{a}}$  and  $p_{\text{w}}^{\text{c}}$  the water partial pressures of the anode and cathode. The rate of water production is simply given by

$$F_{\text{w,product}} = \frac{iA}{2F} \quad (4)$$

Relative ratios of water carried away by hydrogen ( $R_{\text{w}}^{\text{a}} = F_{\text{w,out}}^{\text{a}}/F_{\text{w,product}}$ ) and air ( $R_{\text{w}}^{\text{c}} = F_{\text{w,out}}^{\text{c}}/F_{\text{w,product}}$ ) streams and water stored in MEA ( $R_{\text{MEA}} = 1 - R_{\text{w}}^{\text{a}} - R_{\text{w}}^{\text{c}}$ ) are shown in Fig. 10. Here it is assumed that hydrogen and air leave the cell at the relative humidity of 50 and 100%, respectively. It is seen from Fig. 10 that 80.5% of product water remains in the cell during startup from  $-1\text{ }^{\circ}\text{C}$ . This means that there is  $0.90\text{ mg/cm}^2$  (i.e.  $1.12 \times 80.5\%$ ) water accumulated in the MEA when the product water reaches  $1.12\text{ mg/cm}^2$ . Since the maximum water storage capacity of the cathode CL and membrane combined is estimated to be  $0.85\text{ mg/cm}^2$ , one may well expect product water to emerge from the CL at this moment.

Rough estimates shown in Fig. 10 indicate that the majority of product water remains in the cell during cold start of automotive PEFCs, and that this amount increases with decreasing startup temperature.

The state of water on the CL surface was further studied in the startup experiment from  $-3\text{ }^{\circ}\text{C}$ . All other conditions remained the same as that from  $-1\text{ }^{\circ}\text{C}$ . The corresponding images are

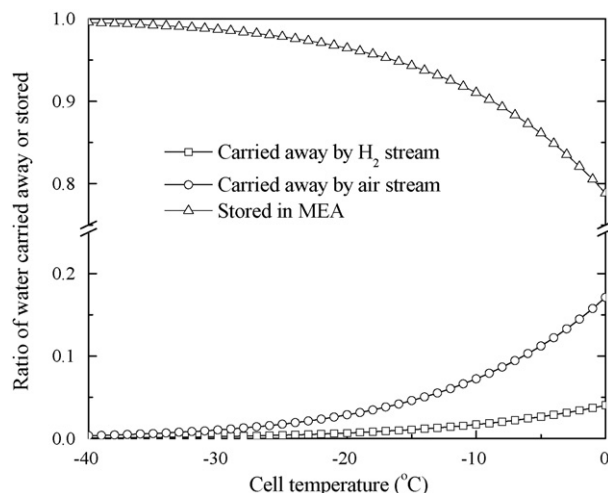


Fig. 10. Relative ratios of water carried away by the exhaust gases and stored in MEA ( $\xi_{\text{H}_2} = 14.35$ ,  $\xi_{\text{air}} = 12.06$ ). It is assumed that hydrogen and air leave the cell at relative humidity of 50 and 100%, respectively.

shown in Fig. 11. It is seen that when the cumulative product water is less than  $0.84 \text{ mg/cm}^2$  as occurred at 90 s into cold start, neither ice/frost nor liquid water is observed. However, when the cumulative product water reaches  $1.12 \text{ mg/cm}^2$ , liquid droplets begins to emerge from the CL. The water droplet diameters are seen to be  $10\text{--}50 \text{ }\mu\text{m}$  and found to grow with time. When the cumulative product water increases to  $2.24 \text{ mg/cm}^2$ , the cell potential drops to  $0.1 \text{ V}$  and the startup operation is terminated, as shown in Fig. 6. In this experiment ( $T = -3 \text{ }^\circ\text{C}$ ,  $p_w^a = 238.03$ ,  $p_w^c = 476.06 \text{ Pa}$ ,  $\xi_{\text{H}_2} = 14.35$ ,  $\xi_{\text{air}} = 12.06$ ), 83.5% of product water is stored in MEA, according to Fig. 10. This leaves  $0.94 \text{ mg/cm}^2$  water accumulated in the MEA when the product water reaches  $1.12 \text{ mg/cm}^2$ . As analyzed earlier, the theoretical capacities of water accumulation in the cathode CL and membrane add up to be  $0.85 \text{ mg/cm}^2$ . Therefore, it is reasonable that product water begins to emerge on the CL surface when the product water reaches  $1.12 \text{ mg/cm}^2$ , as visually captured by the images. Once again, the water observed on the CL surface in the startup from  $-3 \text{ }^\circ\text{C}$  is liquid, due to either the temperature difference between the cell plate and the cathode CL or a minor degree of freezing-point depression of water within CL pores.

The images on CL surface during startup from lower temperatures (i.e.  $T_{\text{cell}} = -4, -5, -10, -15$ , and  $-20 \text{ }^\circ\text{C}$ ) are much different from those at  $-3$  and  $-1 \text{ }^\circ\text{C}$ , where no water droplets, frost or ice can be observed on the CL surface at any time. That is, there is no water emerging out of the cathode CL. The surfaces of GDL, current-collecting lands and flow channels were also carefully checked by an optical microscope with no water, frost or ice found. During the cold-start experiment from  $-4 \text{ }^\circ\text{C}$ , the cumulative product water at shutdown is only  $0.93 \text{ mg/cm}^2$ . Considering 84.9% of that product water is stored in MEA according to Fig. 10, this is  $0.79 \text{ mg/cm}^2$  water accumulated in the catalyst layer and membrane, apparently unable to exceed the theoretical capacity before water can emerge from the CL and hence supporting the observation that no water is detected on the CL surface (no shown here). As shown in Fig. 4, the initial water content of the membrane is 6.0 after the cell is purged with dry

gases for 120 s. Hence  $0.47 \text{ mg/cm}^2$  water can be stored in a membrane of  $18 \text{ }\mu\text{m}$  thickness if the membrane water content is raised from 6 initially to 14 at full hydration [16]. A comparison of the product water achieved at shutdown (i.e.  $0.37 \text{ mg/cm}^2$  at cold-start temperature of  $-20 \text{ }^\circ\text{C}$ ) to the theoretical water storage capacity of the membrane (i.e.  $0.47 \text{ mg/cm}^2$ ) implies that product water does not fully diffuse into and hydrate the entire membrane.

To further confirm that what was observed on the CL surface as shown in Figs. 9c and d and 11c–f is liquid water but not ice or frost, a “quenching” experiment was carried out after the startup from  $-3 \text{ }^\circ\text{C}$  by turning off the current load, shutting off the inlet and outlet gases and maintaining cell temperature at  $-3 \text{ }^\circ\text{C}$  for 2 h. Through this process, the liquid water underwent phase transition from liquid to ice/frost on the CL surface, as shown in Fig. 12. Fig. 12a displays the water droplets generated during cold start at  $-3 \text{ }^\circ\text{C}$ , and Fig. 12b shows the ice particles frozen from the same water droplets. Water droplets and ice particles on the CL surface differ in shape: the droplets appear round, while the ice particles are irregular. This “quenching” experiment confirms that it is liquid water to emerge from CL surface in startup experiments from  $-1$  and  $-3 \text{ }^\circ\text{C}$ , but not ice.

### 3.5. Freezing-point depression of water in catalyst layer

An interesting experiment was carried out to separate actual freezing-point depression of water in the CL from the temperature difference between the land and CL during cold start. Here, the freezing-point depression due to the effect of well-known Gibbs-Thomson undercooling [27],  $\Delta T_{\text{FPD}}$ , defined as the difference between the freezing point in small pores and the normal equilibrium temperature of water,  $T_E$  (i.e.  $273.15 \text{ K}$ ), is inversely proportional to the pore radius

$$\Delta T_{\text{FPD}} = \frac{\sigma_{\text{LS}} T_E \cos \alpha}{\rho_s h_{\text{fg}} r_{\text{CL}}} \quad (5)$$

where  $\sigma_{\text{LS}}$  the surface tension of ice-water interface ( $\text{J/m}^2$ ),  $\alpha$  the contact angle,  $\rho_s$  and  $h_{\text{fg}}$  the ice density ( $\text{kg/m}^3$ ) and latent heat of fusion ( $\text{J/kg}$ ), and  $r_{\text{CL}}$  the pore radius of the catalyst layer. Clearly, the freezing point of water is lowered in confined spaces as the size decreases. Much of the knowledge on ice formation in confined spaces and its ensuing damage to the matrix structure is available in cryobiology [28,29].

It is noted that the rate of total heat generated in the cell can be described by  $(U_0 - T \partial U_0 / \partial T - V_{\text{cell}}) i A$  and most of heat is generated in the cathode CL and membrane [30]. Here  $U_0$  is thermodynamic potential and  $V_{\text{cell}}$  cell potential. In this work, the flow rates of reactant gases exiting the cell are very low ( $F_{\text{H}_2, \text{out}} = 3.458 \times 10^{-5} \text{ mol/s}$ ,  $F_{\text{air, out}} = 7.307 \times 10^{-5} \text{ mol/s}$  @  $i = 0.1 \text{ A/cm}^2$ ). Heat capacity of hydrogen and air are  $28.84$  and  $29.20 \text{ J/mol K}$ , respectively [31]. If we assume that the temperature difference between inlet and outlet gases amounts to  $2.5 \text{ }^\circ\text{C}$ , the rate of heat removal by gases is only  $7.83 \times 10^{-3} \text{ W}$  as compared to  $0.29 \text{ W}$  heat generation under typical operating conditions ( $V_{\text{cell}} = 0.66 \text{ V}$ ,  $i = 0.1 \text{ A/cm}^2$ ). Thus, it can be concluded that the heat removed by gases is negligible and heat

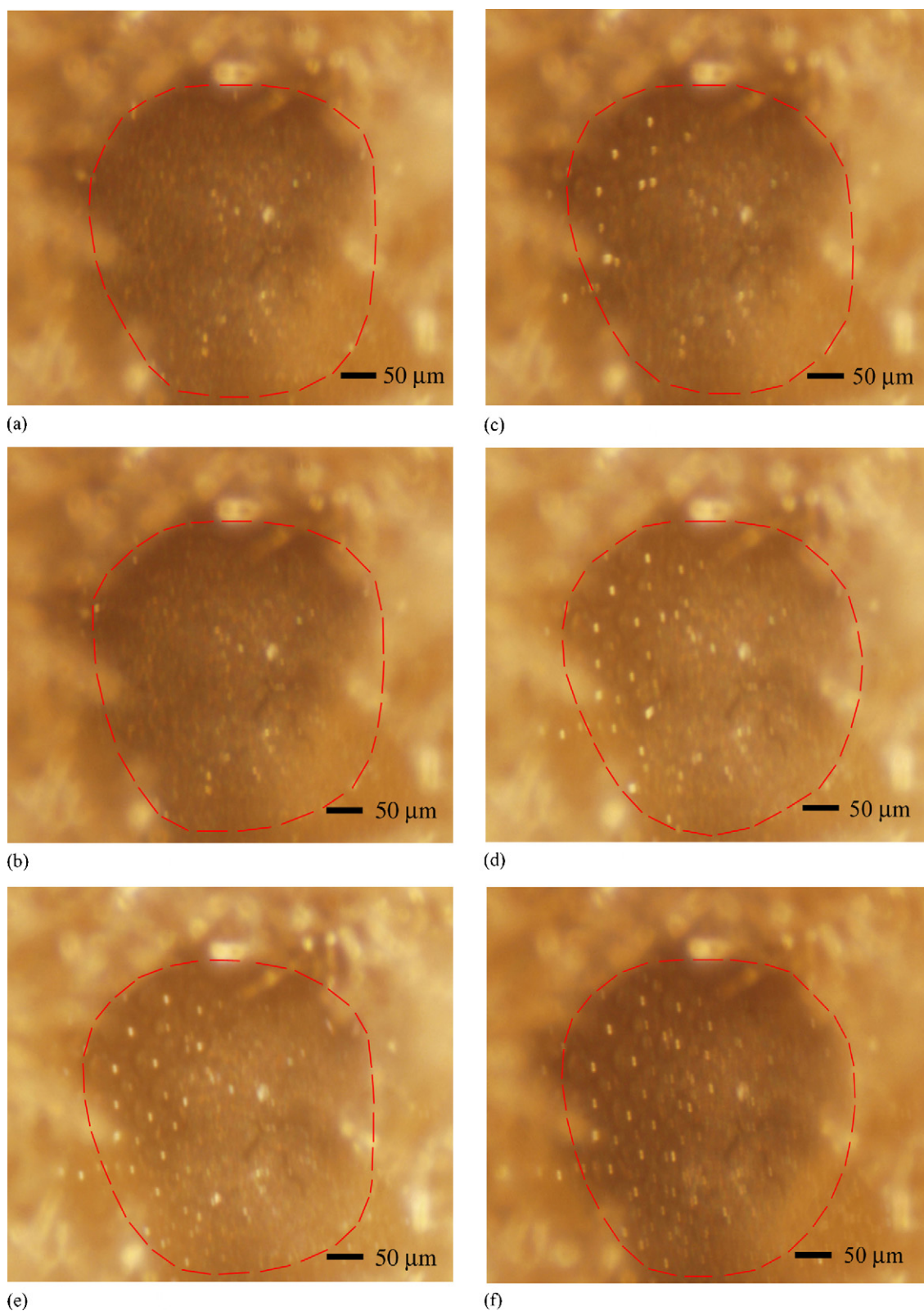
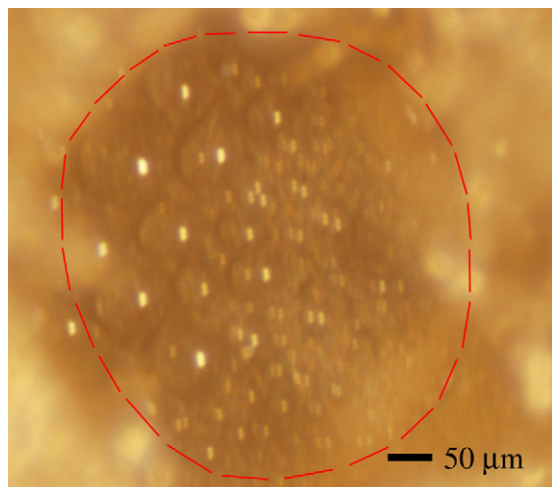
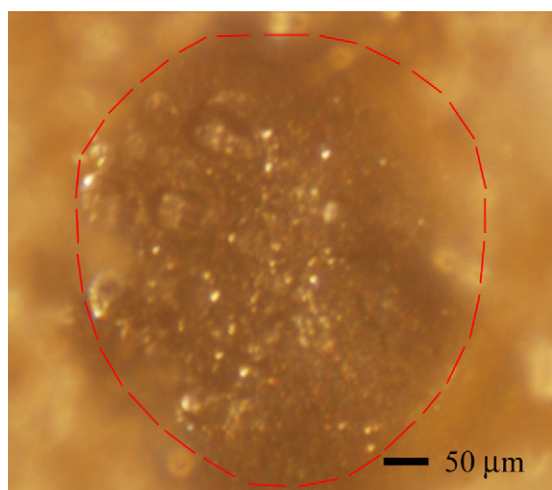


Fig. 11. Images on the CL surface during startup from  $-3\text{ }^{\circ}\text{C}$  (purge conditions are  $T_{\text{purge}} = 55\text{ }^{\circ}\text{C}$ ,  $t_{\text{purge}} = 120\text{ s}$ , and startup conditions are  $T_{\text{cell}} = -3\text{ }^{\circ}\text{C}$ ,  $i = 0.1\text{ A/cm}^2$ ,  $\xi_{\text{H}_2} = 14.35$ ,  $\xi_{\text{air}} = 12.06$ ,  $\text{RH}_{\text{H}_2} = \text{RH}_{\text{air}} = 0\%$ ,  $p_{\text{H}_2} = p_{\text{air}} = 1\text{ atm}$ ). (a)  $m_w = 0\text{ mg/cm}^2$ , (b)  $m_w = 0.84\text{ mg/cm}^2$ , (c)  $m_w = 1.12\text{ mg/cm}^2$ , (d)  $m_w = 1.40\text{ mg/cm}^2$ , (e)  $m_w = 1.96\text{ mg/cm}^2$  and (f)  $m_w = 2.24\text{ mg/cm}^2$ .



(a)



(b)

Fig. 12. Phase transition from water droplets to ice particles. Water droplets were generated during cold start from  $-3^{\circ}\text{C}$  and observed on the CL surface. Then the cell was left open circuit at  $-3^{\circ}\text{C}$  for 2 h, in which period the water droplets turned into ice particles. (a) Water droplets and (b) ice particles.

generated in the CL and membrane is primarily removed through the GDL (with MPL) to the end plate. In all experiments in this work, the temperature of the end plates is kept constant at the startup temperature. The temperature increase ( $\Delta T = T_{\text{CL}} - T_{\text{end plate}}$ ) in the cathode CL then depends on current density and cell potential. In contrast, freezing-point depression of water in the porous CL ( $T_{\text{FPD}}$ ) should not vary with current density.

On basis of this reasoning, additional experiments were carried out by varying the current density during cold start. Fig. 13 shows cell voltage curves for startup from  $-2$  to  $-1^{\circ}\text{C}$  and at the current density of  $0.02\text{ A/cm}^2$ . The purge conditions are the same as in experiments shown in Fig. 5. Dry hydrogen and air were fed to the cell at stoichiometric ratios of 14.35 and 12.06 @  $i = 0.02\text{ A/cm}^2$  ( $\text{H}_2$  flow rate: 10 ml/min, STP; air flow rate: 20 ml/min, STP), respectively. Similar to the cold-start operation at the current density of  $0.1\text{ A/cm}^2$ , the cell can operate indefinitely when the cell is started up from  $-1^{\circ}\text{C}$  at the current

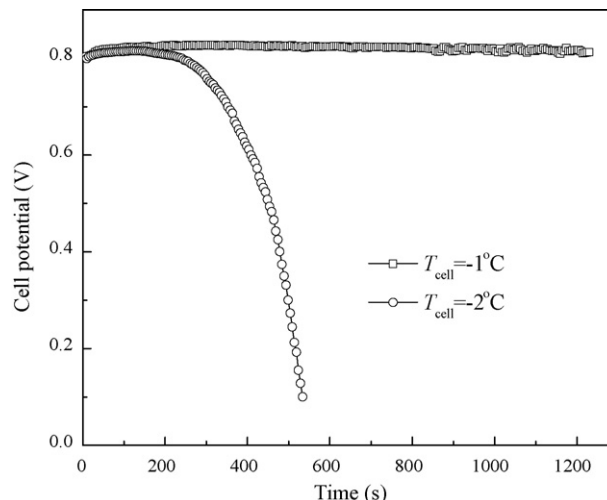


Fig. 13. Cell voltage curves for startup from  $-2$  and  $-1^{\circ}\text{C}$  (purge conditions are  $T_{\text{purge}} = 55^{\circ}\text{C}$  and  $t_{\text{purge}} = 120\text{ s}$ , and startup conditions are  $i = 0.02\text{ A/cm}^2$ ,  $\xi_{\text{air}} = 12.06$ ,  $\xi_{\text{H}_2} = 12.06$ ,  $\text{RH}_{\text{H}_2} = \text{RH}_{\text{air}} = 0\%$ ,  $p_{\text{H}_2} = p_{\text{air}} = 1\text{ atm}$ ).

density of  $0.02\text{ A/cm}^2$ . While starting from  $-2^{\circ}\text{C}$ , the cumulative product water at shutdown is  $1.00\text{ mg/cm}^2$ . Since 82.1% of product water is stored in MEA according to Fig. 10, this is  $0.82\text{ mg/cm}^2$  water accumulated in the MEA. This value is lower than the theoretical water storage capacity of the membrane and cathode CL combined (i.e.  $0.85\text{ mg/cm}^2$ ). Thus, it can be deduced that water is ice in the CL during  $0.02\text{ A/cm}^2$  startup from  $-2^{\circ}\text{C}$ , but liquid water in the CL during startup from  $-1^{\circ}\text{C}$ . It follows that the value of  $(\Delta T + \Delta T_{\text{FPD}})$  @  $i = 0.02\text{ A/cm}^2$  should be lower than  $2^{\circ}\text{C}$ , but higher than  $1^{\circ}\text{C}$ . Similarly, the value of  $(\Delta T + \Delta T_{\text{FPD}})$  @  $i = 0.1\text{ A/cm}^2$  should be lower than  $4^{\circ}\text{C}$  but higher than  $3^{\circ}\text{C}$ . Mathematically one has

$$\Delta T_{0.1} + \Delta T_{\text{FPD}} = 3.5 \pm 0.5 \quad (6)$$

$$\Delta T_{0.02} + \Delta T_{\text{FPD}} = 1.5 \pm 0.5 \quad (7)$$

where  $\Delta T_{0.1}$  and  $\Delta T_{0.02}$  are the temperature differences between cathode CL and end plate when the cell is operated at 0.1 and  $0.02\text{ A/cm}^2$ , respectively. Since the rate of heat generation at  $0.1\text{ A/cm}^2$  is roughly five times of that at  $0.02\text{ A/cm}^2$ , one may expect

$$\Delta T_{0.1} = 5\Delta T_{0.02} \quad (8)$$

Solving Eqs. (6–8) yields  $\Delta T_{\text{FPD}} = 1.0 \pm 0.5^{\circ}\text{C}$  and  $\Delta T_{0.1} = 2.5 \pm 0.5^{\circ}\text{C}$ . This estimate of the freezing-point depression, while numerically more exact than that analyzed in Ge and Wang [16], reaches the same conclusion that freezing-point depression should be negligible in cold-start theory and practice for the startup temperature range between  $-20$  and  $-30^{\circ}\text{C}$  of interest for automotive applications.

The analysis described above also indicates that the temperature difference between the CL and end plate is approximately  $25^{\circ}\text{C cm}^2/\text{A}$ . This value is higher than experimental data and simulation results reported in the literature under normal temperatures. For example, Vie and Kjelstrup [32] reported that the temperature difference between two sides of GDL is  $5^{\circ}\text{C}$  when the cell is operated at  $1\text{ A/cm}^2$  (with the average temperature at

73 °C). The simulation results of Ju et al. [33] showed that the temperature difference between CL and end plate is 11 °C when the cell is operated at 0.7985 A/cm<sup>2</sup> at the average temperature of 87.2 °C and if the thermal conductivity of GDL is assumed to be 0.5 W/mK. This is a temperature difference of 13.8 °C cm<sup>2</sup>/A. Two possible reasons for higher temperature difference between the CL and end plate at subzero temperatures are: (1) lower GDL thermal conductivity at subzero temperatures than at ~80 °C; and (2) larger thermal contact resistance at subzero temperatures due perhaps to ice formation at the CL and MPL/GDL interface.

#### 4. Conclusions

We have examined a complete set of events centering on PEFC cold start, starting from gas purge, to cool down, to subzero startup, and finally to warm up. We describe a simple method to visualize water/ice formation on the CL surface in an operating PEFC, enabling elucidation of water transport in the subzero environment. Gas purge is found to be a key step to ensure self-startup from subzero temperatures. Purge duration of 120 s using dry gas appears to be optimal. After gas purge there is substantial relaxation of membrane HFR over a period of longer than 30 min, indicating water redistribution within the MEA. Understanding the precise mechanisms for HFR relaxation merits future study.

Following gas purge, the membrane HFR exhibits smooth rise with decreasing temperature during cool down, except when the membrane is nearly fully hydrated. This is indicative of no phase transition of water within membranes of practical interest in the startup of automotive fuel cells. As expected, cold-start performance depends strongly on the purge duration and startup temperature. However, their nonlinear relationships unraveled in this work are significant.

The state of water in the cathode CL has been carefully examined by direct observations in an operating PEFC as well as water balance analysis. Freezing-point depression of water in the CL is found to be  $1.0 \pm 0.5$  °C, which is sufficiently small to be neglected in cold-start theory and practice for the startup temperature range between –20 and –30 °C of interest in automotive applications.

#### Acknowledgments

Financial support of this work by Nissan Motor Co. Ltd is acknowledged. The authors are grateful to Dr. Feng-Yuan Zhang who developed the method of using gas diffusion layers punched with microholes to visualize water dynamics in a number of projects at ECEC over last several years and assisted in preparing the GDL used in this work. We also thank Y. Tabuchi and K.

Yoshizawa of Nissan and K. Tajiri and L. Mao of ECEC for many useful discussions.

#### References

- [1] R.C. McDonald, C.K. Mittelsteadt, E.L. Thompson, *Fuel Cells* 4 (2004) 208.
- [2] M.S. Wilson, J.A. Valerio, S. Gottesfeld, *Electrochim. Acta* 40 (1995) 355.
- [3] E.A. Cho, J.J. Ko, H.Y. Ha, S.A. Hong, K.Y. Lee, T.W. Lim, I.H. Oh, *J. Electrochem. Soc.* 150 (2003) A1667.
- [4] E.A. Cho, J.J. Ko, H.Y. Ha, S.A. Hong, K.Y. Lee, T.W. Lim, I.H. Oh, *J. Electrochem. Soc.* 151 (2004) A661.
- [5] Q. Guo, Z. Qi, *J. Power Sources* 160 (2006) 1269.
- [6] J. St-Pierre, J. Roberts, K. Colbow, S. Campbell, A. Nelson, *J. New Mater. Electrochem. Syst.* 8 (2005) 163.
- [7] F. Kagami, Y. Hishinuma, T. Chikahisa, *Thermal Sci. Eng.* 10 (2002) 25.
- [8] Y. Hishinuma, T. Chikahisa, F. Kagami, T. Ogawa, *JSME Int. J. Series B* 47 (2004) 235.
- [9] M. Oszcipok, D. Riemann, U. Kronenwett, M. Kreideweis, M. Zedda, *J. Power Sources* 145 (2005) 407.
- [10] M. Oszcipok, M. Zedda, D. Riemann, D. Geckeler, *J. Power Sources* 154 (2006) 404.
- [11] L. Mao, K. Tajiri, S.H. Ge, X.G. Yang, C.Y. Wang, Abstract 998, The Electrochemical Society Meeting Abstracts, vol. 2005-2, Los Angeles, CA, Oct. 16–21, 2005.
- [12] M. Cappadonia, J.W. Erning, S.M.S. Niaki, U. Stimming, *Solid State Ionics* 77 (1995) 65.
- [13] M. Cappadonia, J.W. Erning, U. Stimming, *J. Electroanal. Chem.* 376 (1994) 189.
- [14] M. Saito, K. Hayamizu, T. Okada, *J. Phys. Chem. B* 109 (2005) 3112.
- [15] E.L. Thompson, T.W. Capehart, T.J. Fuller, J. Jorne, *J. Electrochem. Soc.* 153 (2006) A2351.
- [16] S.H. Ge, C.Y. Wang, *Electrochem. Solid-State Lett.* 9 (2006) A499.
- [17] L. Mao, C.Y. Wang, *J. Electrochem. Soc.* 154 (2007) B139.
- [18] L. Mao, C.Y. Wang, Y. Tabuchi, *J. Electrochem. Soc.* 154 (2007) B341.
- [19] K. Tajiri, Y. Tabuchi, C.Y. Wang, *J. Electrochem. Soc.* 154 (2007) B147.
- [20] K. Tajiri, Y. Tabuchi, F. Kagami, S. Takahashi, K. Yoshizawa, C.Y. Wang, *J. Power Sources* 165 (2007) 279.
- [21] Y. Ishikawa, T. Morita, K. Nakata, K. Yoshida, M. Shiozawa, *J. Power Sources* 163 (2007) 708.
- [22] P. Berg, K. Promislow, J. St. Pierre, J. Stumper, B. Wetton, *J. Electrochem. Soc.* 151 (2004) A341.
- [23] S.H. Ge, X.G. Li, B.L. Yi, I.M. Hsing, *J. Electrochem. Soc.* 152 (2005) A1149.
- [24] H. Ju, C.Y. Wang, S. Cleghorn, U. Beuscher, *J. Electrochem. Soc.* 152 (2005) A1645.
- [25] X. Ye, C.Y. Wang, *J. Electrochem. Soc.* 154 (2007) in press.
- [26] T.E. Springer, T.A. Zawodzinski, S. Gottesfeld, *J. Electrochem. Soc.* 138 (1991) 2334.
- [27] W. Kurz, D.J. Fisher, *Fundamentals of Solidification*, Trans. Tech. Publications, Switzerland, 1984, 13.
- [28] M. Toner, E.G. Cravalho, M. Karel, *J. Appl. Phys.* 67 (1990) 1582.
- [29] J.P. Acker, J.A.W. Elliott, L.E. McGann, *Biophys. J.* 81 (2001) 1389.
- [30] C.Y. Wang, *Chem. Rev.* 104 (2004) 4727.
- [31] D.R. Lide (Ed.), *CRC Handbook of Chemistry and Physics*, 77th ed., CRC Press, Boca Raton, FL, 1997.
- [32] P.J.S. Vie, S. Kjelstrup, *Electrochim. Acta* 49 (2004) 1069.
- [33] H. Ju, H. Meng, C.Y. Wang, *Int. J. Heat Mass Transfer* 48 (2005) 1303.